Marine Pollution Bulletin 100 (2015) 70–81

Contents lists available at ScienceDirect

Marine Pollution Bulletin

journal homepage: www.elsevier.com/locate/marpolbul

Abundance, size and polymer composition of marine microplastics ≥10 μm in the Atlantic Ocean and their modelled vertical distribution

Kristina Enders *, Robin Lenz, Colin A. Stedmon, Torkel G. Nielsen

National Institute of Aquatic Resources, Technical University of Denmark, DTU, Kavalergården 6, 2920 Charlottenlund, Denmark

ARTICLE INFO

Article history:
Received 21 July 2015
Received in revised form 8 September 2015
Accepted 15 September 2015
Available online 9 October 2015

Keywords:
Small microplastic
Continuous monitoring
Horizontal distribution
Size-selective vertical distribution
Model

ABSTRACT

We studied abundance, size and polymer type of microplastic down to 10 μm along a transect from the European Coast to the North Atlantic Subtropical Gyre (NASG) using an underway intake filtration technique and Raman micro-spectrometry. Concentrations ranged from 13 to 501 items m^{-3}. Highest concentrations were observed at the European coast, decreasing towards mid-Atlantic waters but elevated in the western NASG. We observed highest numbers among particles in the 10–20 μm size fraction, whereas the total volume was highest in the 50–80 μm range. Based on a numerical model size-dependent depth profiles of polyethylene microspheres in a range from 10–1000 μm were calculated and show a strong dispersal throughout the surface mixed layer for sizes smaller than 200 μm. From model and field study results we conclude that small microplastic is ubiquitously distributed over the ocean surface layer and has a lower residence time than larger plastic debris in this compartment.

1. Introduction

The presence of plastic debris in marine environments has been recognised as a global problem (Andrady, 2003; Ivar do Sul and Costa, 2014; Rocha-Santos and Duarte, 2014). Predictions of the amount of plastic floating in the ocean are on the order of 250,000 tons (Eriksen et al., 2014), which is more than an order of magnitude lower than conservative estimates of annual plastic waste input, which was between 4.8–12.7 million tons in 2010 (Jambeck et al., 2015). Given that plastics became a disposable mass product in the 1950s and production increased steadily since, there is a large fraction of plastic waste which is unaccounted for.

Once in the oceans plastic undergoes gradual degradation into smaller fragments via physical, chemical and biological processes (Andrady, 2011). Common terms used to categorise plastic debris by its size, are macro, meso-, micro- and nanoplastics. However, no standard boundaries have been implemented (Costa et al., 2010; Cole et al., 2011; Andrady, 2011). For microplastic, many use a lower size limit of approximately 300 μm (Law et al., 2010; Rocha-Santos and Duarte, 2014; Magnusson, 2013). We refer to this fraction as large microplastic (L-MP) and to particles smaller than that as small microplastic (S-MP), the latter being the major subject of the present study. The size distribution and therefore availability to different groups of organisms depends on degradation and distribution processes.

Plastics are a transport vector of persistent organic pollutants (POP) and heavy metals as well as a source of chemical pollutants themselves such as phthalate plasticisers, polybrominated diphenyl ether flame retardants (PBDE) and bisphenols (Rochman, 2013) While large plastic debris is a concern mainly due to physical harm, MP fragments additionally have an increased risk due to their larger surface to volume ratio. This results in higher adsorption capacities (Lee et al., 2014) which, in combination with higher bioavailability makes them a potential carrier of pollutants into the food web (Avio et al., 2015). Several laboratory studies indicate toxicological risks of S-MP but concentrations in nature are not well known and only few studies exist (Norén and Naustvoll, 2011; Norén et al., 2014; Desforges et al., 2014).

The S-MP covers the food size range of zooplankton, where copepods constitute the major group (Boyd, 1976). They form the link to planktivorous fish and thereby can be an entrance for pollutants to the food chain. Studies demonstrated uptake and a competing effect of microplastic with nutritious food and subsequent loss of energetic resources, showing sub-lethal effects in egg production and reproductive output (Cole et al., 2013; Cole et al., 2015).

The purpose of this study was to investigate the distribution of S-MP from coastal waters to the open ocean. For future studies on microplastic–zooplankton interactions, it is essential to know the concentration that organisms are exposed to in nature. To reconstruct the fate of MP we need to understand the underlying dynamics in the marine plastic circulation. The horizontal transport of buoyant plastics is mainly determined by currents, induced by wind forcing and geostrophic circulation. This becomes obvious from the observations and model predictions that show highest concentrations in

* Corresponding author.
E-mail address: kren@aqua.dtu.dk (K. Enders).

http://dx.doi.org/10.1016/j.marpolbul.2015.09.027
0025-326X/

coastal waters and the subtropical convergence zones of the sea surface velocity field (Isobe et al., 2014; Law et al., 2010; Cózar et al., 2014). In the practical part of the present study we investigated the abundance, size and polymer type distribution of microplastics of sizes down to 10 μm in near-surface waters on a transect through different oceanographic regions: coastal waters (Southern North Sea, English Channel, Celtic Sea), the open ocean (Atlantic) and gyre system (Sargasso Sea). It is hypothesised that microplastic concentration is highest in coastal regions then declines with increasing distance, but is elevated within the North Atlantic Subtropical Gyre (NASG). Further, it is investigated if microplastics are associated with distinct water masses and therefore differ across frontal systems. We developed a large-scale sampling method for microplastic down to 10 μm which can be conducted continuously alongside other vessel operations. For the analysis we conducted a study comparing visual identification with Raman micro-spectrometry, which is subject of an accompanying paper (Lenz et al., 2015).

More than half of the produced plastics have a lower density than seawater which makes them passively floating at the ocean's surface where they are subjected to mixing within the surface boundary layer (Kukulka et al., 2012). Vertical distribution is governed by wind-induced turbulences such as breaking surface waves, bubble injection and Langmuir circulations (Kukulka et al., 2012). Studies investigating the vertical distribution of plastic have shown that MP mass decreases faster than particle abundance. This implies size-selective loss terms that preferentially remove S-MP (Reisser et al., 2015; Cózar et al., 2014). Apart from the extrinsic processes named above, the vertical distribution of plastics also depends on intrinsic factors, such as the plastic's density, size and shape, which all together influence its advection velocity, and hence, the ability to maintain its neutrally buoyant position against turbulent displacement (Ballent et al., 2012). Therefore, in the present study we discuss the apparent loss of S-MP from the ocean surface layer using a numerical model that describes the size-selective vertical distribution of low-density microplastic particles through turbulent mixing.

2. Material and methods

2.1. Sample collection

The sampling was conducted alongside the Danish 'Eel Expedition' research cruise onboard R/V DANA from February to April 2014. Without influencing other activities on board, continuous sampling was carried out via the vessel's underway seawater intake connected to a staggered filtering device inside the ship. Sample collection was halted when the vessel stopped for standard cruise sampling stations, in order to avoid contamination. The vessels speed during which the pump was running ranged between 1–2 kn when surveying and 10–12 kn when steaming. Across all analysed stations the average sampling time was 10 ± 5 h. The sample volume was 2.6 ± 1.3 m^3, calculated by flow rate, which was 4.4 ± 1.4 l min^{-1} in average, and sampling time. In total 60 m^3 have been filtered. The seawater intake was located at 3 m below waterline on the forward port side of the vessel. The greywater outlet is situated at the aft starboard side of the ship and does therefore not affect the water collected. Seawater was pumped aboard using a Grundfos CRT 02 pump at 0.37 kW power, 50 Hz with an average flow rate of 2.5 m^3 per hour. It is a vertical non-selfpriming, multistage, centrifugal pump made of titanium and stainless steel. Due to the wave-induced vertical movements of the ship and the hydrodynamic turbulence from the ship bow, the seawater received at the intake is regarded an integral of the first 3 m of the water column. Through stainless steel and food grade polyvinylchloride pipes seawater was directed to the wet laboratory in the ship where the microplastic filtering device was connected, parting the water flow before exiting the ship again. The sampling device which is made of polypropylene pipe modules of 160 mm in diameter

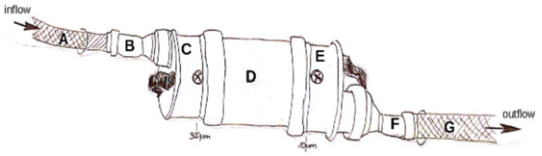

Fig. 1. Sketch of the MP filter unit consisting of (A) inflow hose, (B) adapter, (C) lid with handle and stopper screws to precisely fit the round-cut net. The middle unit (D) holds the two meshes in place, 300 μm and 10 μm (or 50 μm) mesh size, respectively. The following outflow compartments (E), (F) and (G) mirror the inflow parts in reverse order.

containing two round filter mesh (plankton net, material: polyamide-6, KC-Denmark) of 300 and 10 μm mesh size at the base of the rectangle (Fig. 1). High suspended material content in some regions required switching to a 50 μm mesh instead in order to prevent clogging of the filter unit. After each sampling period the valve to the sampling device was closed and the two filter meshes transferred into individual petri dishes, sealed and stored in room temperature until analysis.

The following data was obtained from the underway ship information system: position (GPS), sea surface temperature, salinity and wind velocity. Wind measurements were derived from the shipboard anemometer at 23 m height above mean waterline.

2.2. Contamination prevention

The sampling device and all filter meshes were thoroughly cleaned with deionised and micro-filtrated water (MilliQ, 1.2 μm) before use. At sampling stop the meshes were removed from the filter cartridge, immediately folded, transferred to a petri dish and sealed. In the laboratory, a dress-code of non-plastic material (lab coat, head cover, nitrile gloves) and cleaned work surfaces, washed hands and forearms were measures to prevent contamination from adhering dirt particles. Prior to use, all instruments and vials were cleaned with MilliQ water. All openings of sampling and analysis devices (e.g. filter unit, funnels in the vacuum pump) were covered with aluminium foil when not in use. A thorough evaluation of contamination risk and its importance for in particular S-MP analysis is highly recommended (Norén and Naustvoll, 2011). In the present study control samples were taken in all methodological steps. The first control was to evaluate contamination from the filter unit (from suction) including filters and was done in the beginning of the cruise. For that 30 l of MilliQ water were filtered in duplicate (control I). Every day when rinsing and vacuum filtrating during sample preparation in the laboratory on land, open petri dishes filled with MilliQ water, were placed in direct proximity to the work area, providing a control of potential airborne contamination (control II). Additional controls accounting for contamination during vacuum filtration were taken by vacuum filtrating 0.5 l MilliQ water through the applied membrane filters (control III). Controls were prepared in the same way as the samples, except control II where direct microscopic examination was conducted. During analysis in the Raman microscope the sample is enclosed inside the instrument's housing. It is expected that any system-caused MP contamination would be noticeable by repetitive occurrence of the same kind of particles throughout the sample set.

2.3. Sample preparation

The targeted sizes of MP ≥ 10 μm required an expeditive method with minimal transferring steps to reduce contamination time and prevent loss of particles. In order to be analysed under the microscope the samples were concentrated and in case of high suspended material content

reduced to subsamples. The filter meshes were first dried at 60 °C for 24 h. Each mesh was transferred into a clean screw-top glass jar containing 150 ml of micro-filtrated water with added and micro-filtrated 150 µl sodium dodecylsulfate solution (SDS, 150 g l^{-1}). The tenside removes organic materials from the plastic and prevents adherence to the nylon mesh or jar. The suspension was subsequently sonificated for 20 min in an ultrasonic bath and settled overnight. The supernatant was directly vacuum filtered using 10 µm pore size polyamide or polycarbonate membrane filter, 25 mm in diameter. The residues prepared for visual identification under the optical microscope were analysed in the remaining volume. Whereas for Raman spectrometry prepared residues were vacuum filtered alike the supernatant and in case of high material content reduced using a plankton splitter. The organic material content of the samples was generally very low and mostly degraded after a storage time of several weeks until further processing.

2.4. Laboratory analysis

The overall aim in the analysis was to reliably discriminate plastic from non-plastic material, to categorise with respect to morphology and plastic type, and to measure the size of the present microplastics. A combined method of visual identification and Raman microspectrometric analysis was applied to minimise false-positive (non-plastics recorded as MP) misidentifications.

While all samples were undergoing the criteria-based visual analysis, a subset (15 out of 23 stations) has been additionally analysed using Raman microspectrometry. From this double-analysed data set we grouped similar items based on characteristic appearance properties. Within each of these groups we calculated the ratio between the total number of visually identified MPs and the part that could be confirmed by Raman spectral analysis (Lenz et al., 2015). In samples where only visual analysis was applied, items were grouped into the same categories and the counted number was multiplied with the respective ratios. All reported concentrations were Raman-corrected in that way. Likewise it was necessary to correct for potentially lost particles from stations where a 50 µm mesh was applied instead of 10 µm. The percentage of particles smaller than 50 µm on all regular 10 µm meshes was determined. The amount of particles on 50 µm meshes was subsequently corrected by this percentage in order to compare data from the different stations.

2.5. Light microscopy

Microplastics were visually identified using an epi-illuminated Leitz Laborlux 12 for filters and a transmitted light inverted Nikon Diaphot 200 microscope with 10× and 50× objectives and 10× oculars. Identification was based on morphological features derived from a pilot-study on self-made plastic shreds and literature data (Norén, 2007). Major plastic features are: the absence of repetitive structures indicative of biological origin, homogeneous colouring unless due to transparency, and in case of fibrous forms equal thickness and three-dimensional bending. The creation of the MP identification catalogue was based on visual examination and additionally assisted by the selective conduction of a melting test with a melting point apparatus using a temperature range of 150 to 280 °C (Omega MPS10 Series). Plastic-typic melting behaviour and odour has been observed to identify uncertain particles. Useful applicability of the melting test was limited to particles >50 µm as smaller particles are practically non-transferable and it becomes impossible to detect melting behaviour or odour.

MP objects were categorised into two major groups: fibres and particles. Other studies used further distinction criteria such as films (or sheets) and expanded foams (Song et al., 2015), however, in the investigated size range of the present study and due to the two-dimensionality of the microscopic images, only fibres were visually distinguishable from other particles. For size distribution analysis particles and fibres were measured in length, according to the longest dimension, and width, perpendicular to length. Particle size distribution was calculated as the geometric mean of the first and the second dimension. Fibres are reported in length only.

2.6. Raman micro-spectrometry

Raman spectra were obtained via spectral measurements on a DXR Raman microscope (Thermo Fisher Scientific) with a laser diameter of 0.5 µm and a wavelength of 455 nm. Raman shifted spectra were recorded in the range of 100–3500 cm^{-1} and with a regular exposure time of 20 s, but up to several minutes in single cases of particles that gave poor signal quality. For Raman micro-spectrometry each sample was directly searched on the filter in a grid-like pattern and with 50% filter area coverage. For the search and spectra collection 10-fold and 50-fold magnification objectives (Olympus) were used, respectively. For each particle suspected of being plastic multiple measurements at different spots on the particle ensured the prevention of false signals due to local impurities such as an organic matrix or enclosures of other materials. A library of all major commodity plastic polymers was created and used as reference (Table 1).

Polymers of high spectral similarity were treated as one in the data analysis. All measured particles were photo-documented and saved together with their corresponding spectra.

2.7. Hydrography

From the same underway water system where samples were collected, a surface CTD system (Seabird SBE 21) provided data on temperature and salinity. Grouping of oceanograhic regions according to hydrographic properties and geography (Fig. 2) allowed spatial comparison of MP concentrations. Maps were generated using Ocean Data View (Schlitzer, 2015). Stations from coastal European waters across the Atlantic, European Coastal (E-Co), European Offshore and Azores (E-Off-AZ) and Atlantic Open Ocean (AOO), were characterised by a steady increase in temperature and salinity and regions were mainly separated geographically. The Sargasso Sea as part of the gyre system was grouped into three separate regions, North-NASG (N-NASG), Mid-NASG (M-NASG), South-NASG (S-NASG), characterised by distinct temperatures as the North Atlantic Subtropical Front was crossed. The strength of the frontal system is varying with season and had its strongest manifestation during the time of the expedition (Ullman et al.,

Table 1
Names and abbreviations of polymers used in the spectral identification with its respective densities (Stuart, 2002). Superscript letters indicate polymers that were treated as one group in this study. The mid-line that separates high (HD) and low density (LD) polymers with respect to the density of seawater (1.02–1.029 g cm^{-3}).

Abbr.	Polymer	g cm^{-3}
PP	Polypropylene	0.85–0.92
EVA[a]	Ethylene vinyl acetate	0.92–0.95
LDPE[a]	High density polyethylene	0.89–0.93
HDPE[a]	High density polyethylene	0.94–0.98
(E)PS[b]	(Expanded) polystyrene	1.04–1.06
ABS[b]	Acrylonitrile butadiene styrene	1.04–1.08
PA	Polyamide	1.12–1.15
PMMA	Polymethylmethacrylate	1.16–1.20
PC[c]	Polycarbonate	1.20–1.22
PU	Polyurethane	1.20–1.26
PET[c]	Polyethyleneterephthalate	1.38–1.41
PES[c]	Group of polyesters	1.10–1.40
PVC	Polyvinylchloride	1.38–1.41
PTFE	Polytetrafluoroethylene	2.10–2.30

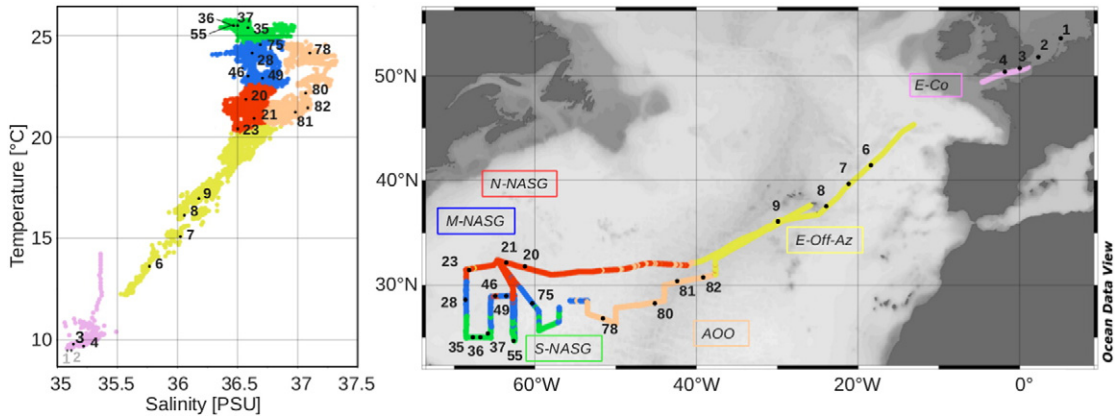

Fig. 2. (left) Temperature-Salinity plot as basis for regional grouping according to hydrographic properties and geography. Stations 1 and 2 are greyed out as no TS-data was available there. (right) Map of regional grouping: European Coastal (E-Co), European Offshore and Azores (E-Off-AZ), Atlantic Open Ocean (AOO), North-NASG (N-NASG), Mid-NASG (M-NASG), and South-NASG (S-NASG).

2007). During the passage the front was located between 25° and 30° north.

2.8. Theoretical fragmentation considerations

Assuming a steady disintegration of large size objects into smaller ones will result in an equal distribution of the total volume V over the number of present size classes n (Cózar et al., 2014). The volume share V_i in each class stays constant and is equal to the product of the single particle volume and the abundance in a class N_i. In case of spherical particles with the diameter d it is given by

$$V_i = \frac{V}{n} = N_i \cdot \frac{\pi d^3}{6}. \quad (1)$$

The number of fragments in a size class then depends on the dimensionality of the break down processes which can be approximated as being three-dimensional for spherical and angular shaped particles, two-dimensional for sheets, films or flakes and one-dimensional for fibres. The numeric distribution of abundance over $i = 1,2,\ldots,n$ size classes can be calculated as

$$N_i = d_i^{-\lambda} \quad (2)$$

where the scaling exponent λ is equal to the dimensionality of the fragmentation process. Hence, number of fibres can be expected to increase inversely with fragment volume, while film and particle abundances scale squared and cubed, respectively.

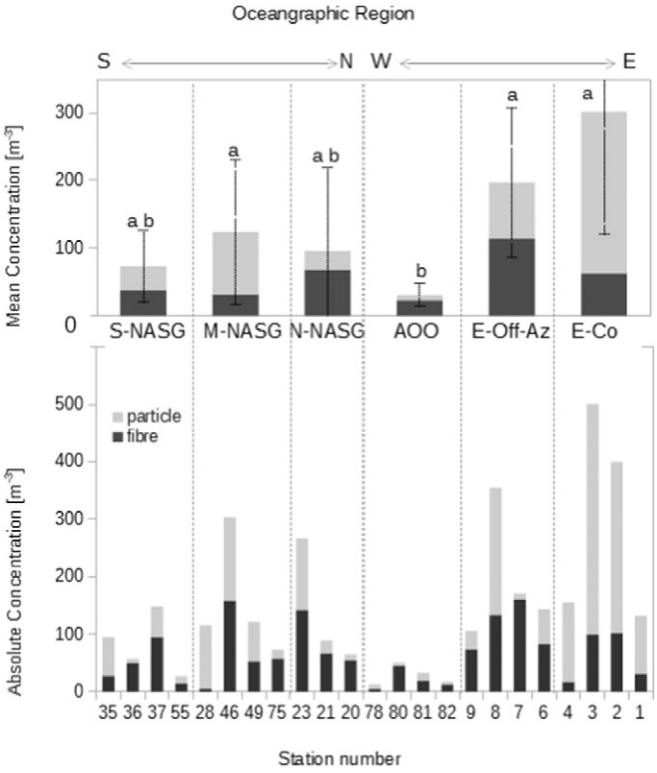

Fig. 3. (top) Averaged concentrations of microplastic particles and fibres grouped in oceanographic regions along the Atlantic transect. Regions not sharing the same letter are significantly different ($p < 0.05$). (bottom) Plastic concentrations for particles and fibres at each measured station. Stations are sorted according to regions in the top panel.

2.9. Statistical analysis

The significance of differences between groups was evaluated using the Mann–Whitney-U test. The Spearman's rank test was used to investigate for the degree of association. Statistics were performed in Matlab (The MathWorks Inc.).

3. Results

3.1. Contamination control

No microplastic particles were found in any of the control steps described in the methods. No particulate plastic resembling material could be found on the blank samples. Few fibres appeared throughout: a total of seven fibres during filtration (control I), a total of 28 fibres were found in control II (number of blanks: n = 10) and two fibres during vacuum filtration (control III). All fibres from all three control steps were, however, of non-plastic nature, suggesting that they originate from non-synthetic clothing worn during laboratory work. Hence all controls were accepted as plastic-free and no quantitative correction of the sample quantification results was applied. Fibres of similar appearance to those in controls have been found in several samples and have been classified as non-plastic.

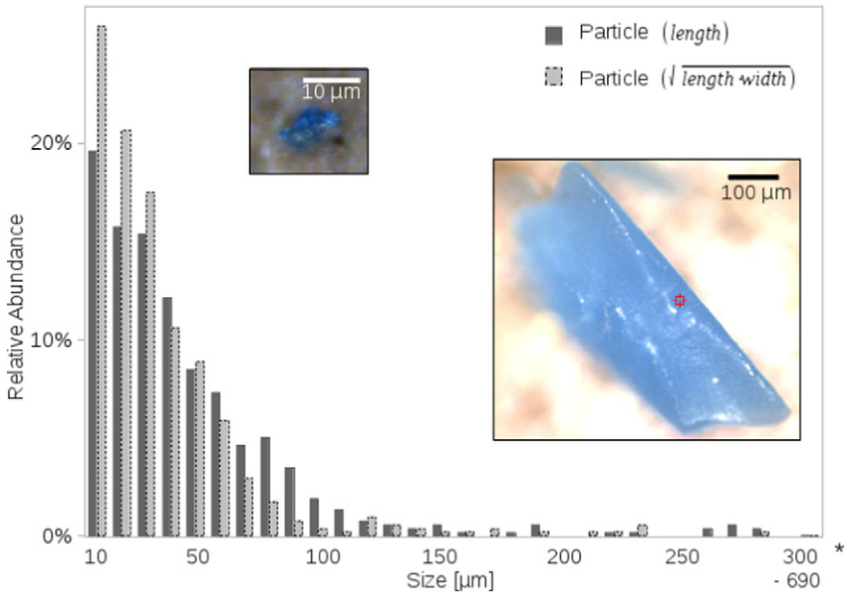

Fig. 4. Relative microplastic particle size distribution of all analysed stations ($n_p = 543$). Dark grey bars represent particles by length. Light grey bars show the size as geometric mean of length and width. The last bar (right) marked with * represents the average of the given size range. Images show the smallest (left) and largest (right) MP particles found and confirmed via Raman-microspectrometry.

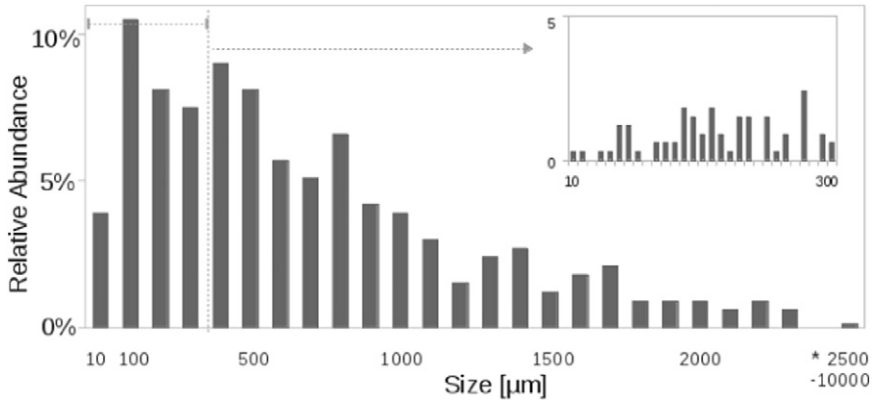

Fig. 5. Relative size distribution of microplastic fibres of all size analysed stations ($n_f = 340$). The last bar (right) marked with * represents the average of the given size range.

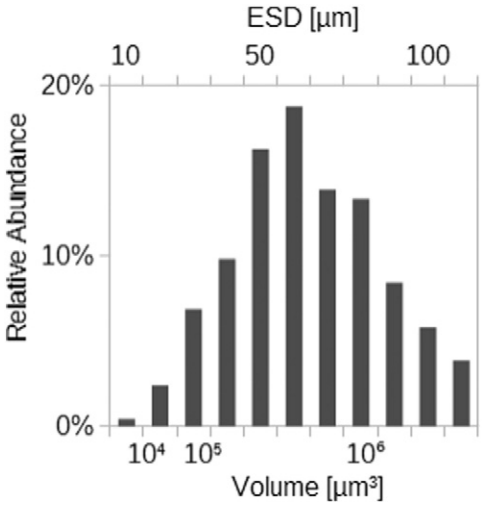

Fig. 6. Plastic volume distribution over equivalent spherical diameter (ESD), approximated by the geometric mean of particle length and width.

3.2. Microplastic abundance

Microplastic was found at all 23 stations with concentrations ranging from 13 to 501 particles m^{-3} (Fig. 3). The total transect length was 4617 km. We observe a strong decreasing trend in average microplastic concentrations on the transect from the E-Co region to the AOO. The average concentrations of microplastic in the E-Co region is significantly higher ($p < 0.05$), nearly 10 times, than concentrations found in the AOO region, which represent the areas of overall highest and lowest MP concentrations, respectively (Fig. 3). The region in between, the E-Off-Az, shows intermediate concentrations with significant differences to the AOO region. E-Off-Az has a local maximum at station 8 where concentrations are more than double of the average of the three other stations in within this region.

From the AOO to the NASG regions the concentrations showed a general increase, with a maximum factor of four comparing AOO to M-NASG. In the NASG, highest concentrations were found in the M-NASG region, which is about 1.7 and 1.3 times the concentrations in S-NASG and N-NASG, respectively. Among the three NASG regions, stations 23 and 46 showed greatest microplastic abundance, on

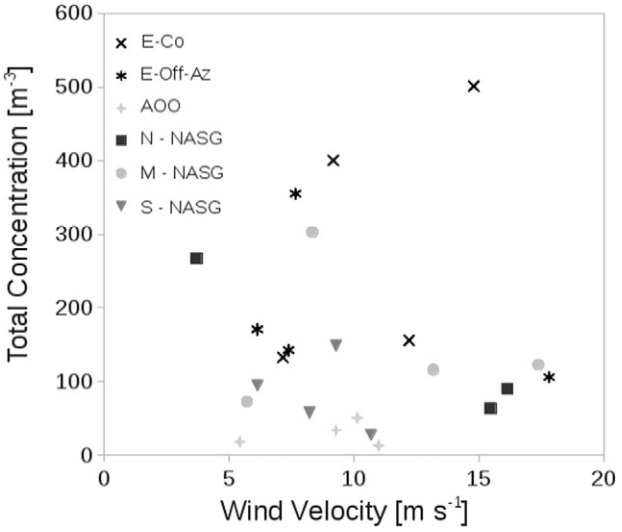

Fig. 7. Total plastic concentration per station, measured via underway water sampling, plotted against average wind speed per station. Data symbols have been assigned to the oceanographic regions.

average three times higher than the mean of the surrounding stations.

Approximately 40% of all microplastics identified was attributed to fibres. Fibrous microplastic concentrations generally follow particle abundance patterns, however the fibre to particle ratio is lower in the E-Co and the M-NASG region with about a third of fibrous MPs. The region of lowest microplastic abundance, AOO, shows highest proportional fibre occurrence. Throughout the transect fibres showed lower spatial fluctuations.

3.3. Microplastic size distribution

The smallest particle and fibre found were 7 μm and 13 μm in length, the largest one 407 μm and 1 cm, respectively ($n_p = 543$, $n_f = 340$). Figs. 4 and 5 show the normalised size distribution of particles and fibres of the size analysed subset ($n = 883$). The majority, 64%, of particles are <40 μm. The same percentage for fibres is reached at <900 μm.

Both particles and fibres were steadily increasing in numbers with decreasing size. The increase in size was, however, lower than what could be expected under continuous fragmentation. Particle size distribution fits a power law regression in the size range from 10 to 110 μm with a scaling exponent of $\lambda = 1.96$ with $r^2 = 0.76$ using the calculated geometric mean size of length and width. Fig. 6 shows the volume distribution of all particle size classes from 10 to 110 μm.

Larger size classes had too small *n* to be compared. Sizes from ≥50 to 80 μm comprise half of the bulk plastic volume for particles in the depicted range. A power law regression fitted to the fibre size distribution and scales with an exponent of $\lambda = 0.999$ with $r^2 = 0.77$, excluding the size range between 10 μm to 100 μm.

Although wind state is known to impact abundance of L-MP and larger plastics in surface samples, in our data there is no trend apparent, neither in the overall nor in within regions (Fig. 7), (Spearman's rank, $r = -0.098$, $p = 0.66$).

3.4. Microplastic characterisation

Approximately half (48%) of the microplastics found were polyethylene (PE) and polypropylene (PP), both having a lower density than seawater (Table 1). The relative contribution of these low density (LD) microplastics shows a rising trend with distance from land (Fig. 8).

In the gyre, the mid region M-NASG shows the highest LD microplastic fraction of approximately 88%. High density (HD) particles such as PS, PA, PMMA, PU, PVC and PES (Table 1) collectively, account for about a quarter of the total. Their contribution is lowest in the M-NASG. Most HD microplastics show a decrease from E-Co to AOO. As an exception, PA, which is relatively equally distributed has its maximum contribution in AOO, the area furthest away from land and with the lowest microplastic load. It is, however, low in absolute abundance in the M-NASG. PES only shows considerable absolute concentrations in the E-Co and E-Off-Az region. PU, which follows a similar but more pronounced decreasing trend with distance from shore is completely absent in the AOO region. PS does not show clear trends in its distribution pattern and is generally very low in abundance. A quarter of the microplastics were assigned to plastic-like polymers (U1). Obtained spectra showed highest similarities with pigments commonly used in textiles and plastics, giving clear indication of their anthropogenic origin. However, the pigment signal completely overlaid the plastic type signal so that a precise identification was not possible. A very low abundant group (U2) was slightly but consistently deviating from U1 and therefore treated as an own group. Properties of these two groups are discussed in the accompanying manuscript (Lenz et al., 2015). Microplastic particles of densities lower than sea water were significantly larger ($p < 0.001$) throughout the transect than those of higher density as can be seen in Fig. 9. This does not hold true for the two fibre categories. However, the low sample sizes for LD fibres question the reliability. LD particles which were predominant in numbers in M-NASG were significantly larger ($p < 0.05$) than in the coastal region. In this region LD and HD

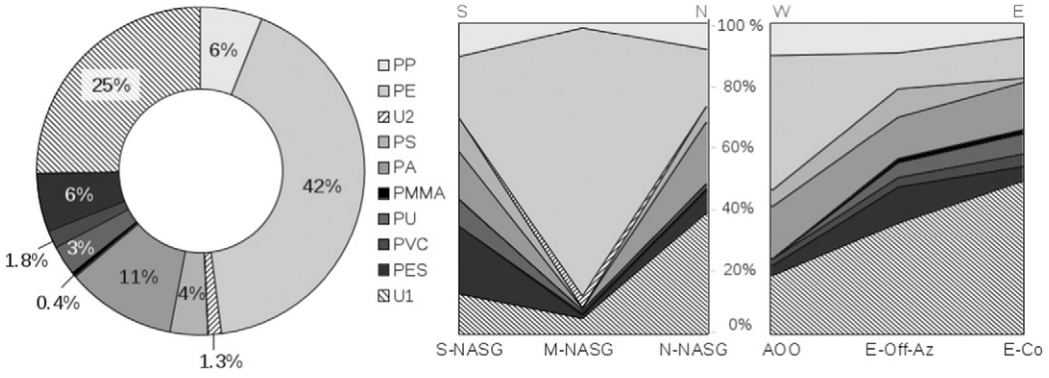

Fig. 8. Relative abundance of polymer types in the Raman confirmed samples from all stations (left) and as transition over the oceanographic regions (right).

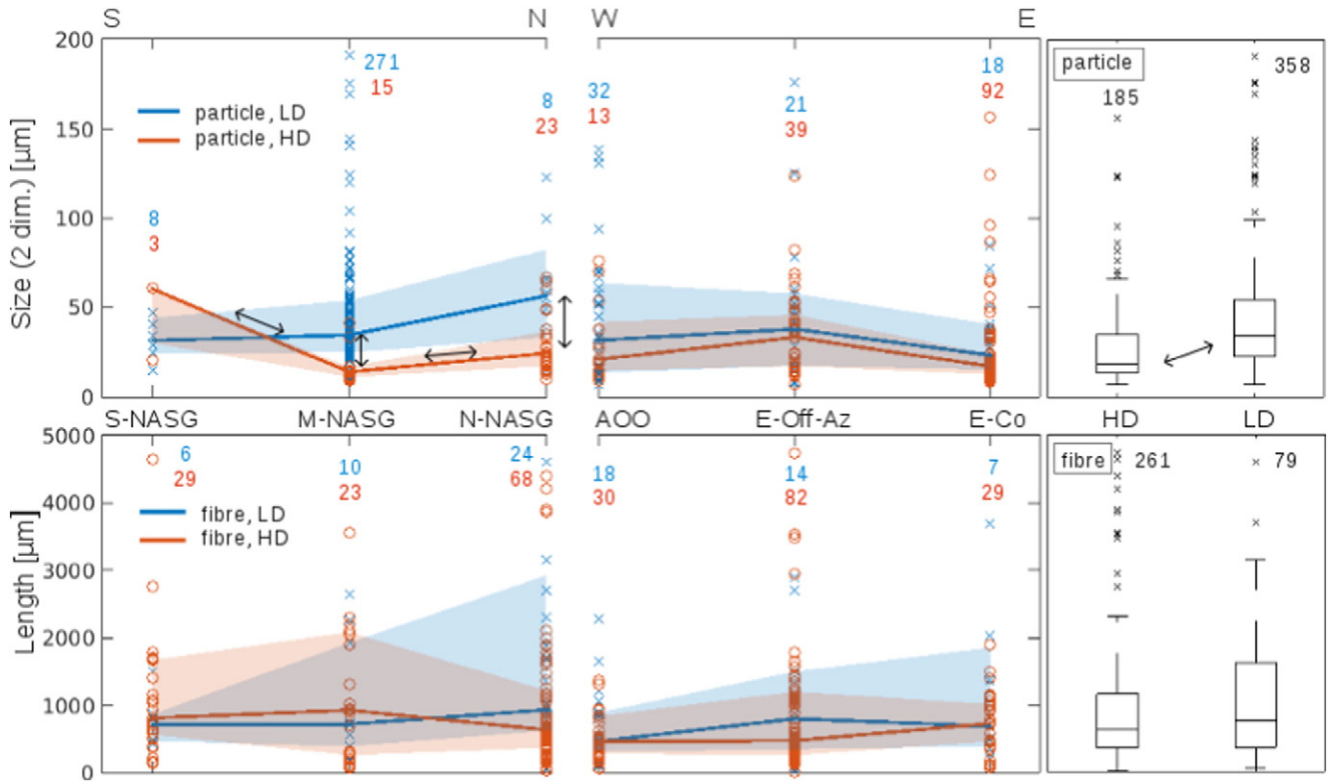

Fig. 9. Distribution of sizes among the oceanographic regions. Particles (top), fibres (bottom). The number of samples *n* for each region is written above the plots. Note: the data shown here is only including the subset of samples that have been Raman-analysed and numbers *n* cannot be related to the total concentrations in the regions. LD polymers are shown in blue, HD polymers in red, following Table 1. The scatter plots (left) are overlaid by the median of the size distribution as a solid line with .25 and .75 quantiles as areas. Arrows indicate significant differences. The box plots (right) compare the total size distribution of lighter and denser polymers. For better visibility y-axes were truncated below the maximum outliers.

particles were significantly different in size ($p < 0.001$). The differences of median sizes were strongest of all regions in the N-NASG and M-NASG with 32 and 21 µm, respectively.

3.5. Model of vertical particle distribution

The vertical distribution of plastic particles in a water column is determined by the advective transport towards neutral buoyancy and turbulent mixing forces that displace particles from their neutral buoyant position. Here we simulate polyethylene with sizes of 10, 100 and 1000 µm. The rising or sinking velocity depends on the difference in density of the polymer (ρ_p = 930 kg m^{-3}) to seawater (ρ_f = 1025 kg m^{-3}) as well as the size and shape of the object in decreasing order of influence (Ballent et al., 2012). The model results are presented in Fig. 10. The shape was approximated to be spherical for all particles by using the equivalent spherical diameter. The terminal velocity w for a sphere with radius r is defined where gravitational force F and the hydrodynamic drag D are equal.

$$F = (m_f - m_p)g = \Delta mg \tag{3}$$

To account for the force of buoyancy, the mass was calculated as the differential mass Δm between the plastic sphere m_p and the water it displaced m_f and g is the gravitational acceleration of 9.81 m s^{-2}.

$$D = \frac{1}{2}\,\pi\, C_D \rho_f r^2 w^2 \tag{4}$$

The drag coefficient C_D is a dimensionless number. An empirical expression for C_D that depends on the Reynolds number was used to calculate the drag force acting on a sphere which is steadily translating through a fluid (Kiørboe et al., 2010).

$$C_D = \frac{24}{Re} + \frac{5}{\sqrt{Re}} + \frac{2}{5} \tag{5}$$

with the Reynolds number Re

$$Re = 2\,\frac{rw}{\nu} \tag{6}$$

where ν is the kinematic viscosity of sea water (here $1.1 \cdot 10^{-6}$ m^2 s^{-1}).

Inserting Eqs. (5) and (6) in Eq. (4) and setting equal to Eq. (3), we get

$$\Delta mg = \frac{1}{2}\,\pi \left(\frac{12\nu}{rw} + \frac{5\sqrt{\nu}}{\sqrt{2rw}} + \frac{2}{5}\right)\rho_f\, r^2 w^2 \tag{7}$$

from which w was implicitly calculated for the three modelled particle sizes.

The spatial solution over a one-dimensional water column with a depth z of 250 m, discretised in spatial layers of 1 m thickness, was solved using an implicit up-wind scheme in closed boundaries according to the partial differential equation

$$\frac{\partial P_i}{\partial t} = \alpha_i \frac{\partial^2 P_i}{\partial z^2} - w_i \frac{\partial P_i}{\partial z} \tag{8}$$

with P_i being the concentration at depth z_i at time t. The mass diffusion coefficient a for turbulent diffusivity was tested in two different cases: firstly, a constant value (0.01 m^2 s^{-1}) and, secondly, a

simulated realistic open ocean diffusivity profile was applied. The latter was obtained from the hydrodynamic model GOTM (Umlauf et al., 2012) using a scenario of ocean weather station data from 'Station Papa' (Burchard et al., 1999). The applied diffusivity profiles are shown in Fig. 10d.

Recently an *in-situ* study demonstrated that numerical plastic concentrations decrease exponentially in within the first 5 m below the air-seawater interface (Reisser et al., 2015). They measured the rising velocities of MP of 500 μm and larger, where smaller plastic particles had lower velocities (lowest 10^{-3}m s^{-1}). This empirical value fits well within the range of the velocities calculated for our model with $5 \cdot 10^{-6}$, $4 \cdot 10^{-4}$ and $2.2 \cdot 10^{-2}$ m s^{-1} for 10, 100 and 1000 μm, respectively.

The largest size group is nearly unaffected by turbulent mixing and 96.5% remains in the first metre from the surface. Particles of 100 μm and 10 μm also have their maximum concentration in the top layer which, however, only account for 4.6% and 1.5% of the total MP abundance in the simulated domain of 250 m. The smallest size class shows nearly uniformly high abundances over the upper 55 m, below which a rapid decrease over 25 m can be observed, asymptotically approaching zero. This coincides with the incipient pycnocline from the simulated hydrodynamic scenario. The total concentration depth distribution is determined by the size spectrum present. The modelled case used the same number of particles for each size class which results in a surface dominated distribution, as shown in Fig. 10f. If a realistic size structure is applied instead where particle numbers increase to the power of 3 with decreasing diameter (Cózar et al., 2014), the total abundance profile will approximate the distribution of the dominant smallest MP classes as shown in Fig. 10g. If volume or mass of plastic were modelled for a pool of fragmented particles instead of size, the bulk will be found accumulating in the surface layer and the combined depth distribution profile will resemble Fig. 10f.

Our model shows that there is a fundamental difference between the vertical dispersion of small and large MP. Positively buoyant polymers like PE and PP of sizes ≥ 1mm are floating on the surface in a similar manner as it is expected for the macroplastic debris they had been fragmented from. Half of the total S-MP of 100 μm is expected to be found in the upper 24 m and there are almost no particles displaced below 56 m (Fig. 10e). For 10 μm the respective depths are 33 and 80 m.

By applying the model to a range of intermediate MP sizes we found a rapid transition from a buoyancy dominated towards a turbulence dominated distribution. The transition was fastest between sizes of 200 to 400 μm. We examined the percentage of particles that were mixed below a surface layer of varying thickness as a measure of the turbulence or advection dominated character (Fig. 11). The calculated Péclet number, which provides an indication of relative importance of diffusivity and advection, ranged from 10^{-10} to 6.5, where only sizes larger 400 μm exceeded $Pe \geq 1$ in the lower parts of the water column. Although the Péclet number suggests a dominance of diffusive transport for all three sizes in the mixed surface layer ($Pe \ll 1$), only a minuscule portion of the 1000 μm particles is dispersed below the surface.

In addition to the described case the model was applied to simulate polystyrene spheres which have a density slightly higher than seawater ($\Delta\rho = 25$ kg m^{-3}, Table 1). While sizes larger 100 μm settled out of the water column relatively quickly, sizes of 10 μm remained mixed throughout the lower half of the modelled domain. Particles approached the lower system boundary asymptomatically over time and no steady state was observed after a maximum simulation length of 40 years.

4. Discussion

Concentrations found in the present study are higher than reported for L-MP (Lusher et al., 2014), however lower in comparison to values found for the same size class (Norén and Naustvoll, 2010; Norén et al., 2014). Our result showed a comparatively low variation over about 1.5 orders of magnitude. The large differences in MP concentrations between studies cannot only be related to the levels of plastic pollution in the investigated regions. Rather it can be explained by different sampling techniques, i.e. surface micro layer, surface layer or subsurface layer sampling, and different mesh sizes. Also the highly dynamic character of the ocean surface compartment creating a temporally and spatially varying patchiness of concentration distributions may contribute to the observed differences.

In offshore waters we found similar concentration levels as a study off the Canadian west coast (Desforges et al., 2014), however, in our study the maximum concentrations in coastal waters were an order of magnitude lower. The averaging effect of our comparatively long individual sampling transects (mean 200 km) combined with the fact that our coastal samples (mid waters of the English Channel) were further away from shore may resulted in this difference. There were no samples in this study that contained zero microplastic suggesting that microplastic is omnipresent. A study of anthropogenic particles and fibres in the Skagerak used a similar methodology, where water from 0–1.5 m below the surface was pumped through a 10 μm polycarbonate pore-filter (Norén and Naustvoll, 2010). Their reported concentrations were more than 2 orders of magnitude higher than our maximum, but included other non-plastic anthropogenic fibres (e.g. semi-synthetic regenerated cellulosic materials) as well as not further specified black particles. It was stated that these can be black carbon, rubber wear from tyres or black minerals misidentified as anthropogenic particles. We also found a large number of black particles that were difficult to identify visually. Only those that exhibited clearly identifiable structural characteristics of MP were included in the data set. Raman analysis of black and transparent particles resulted in a significantly higher rejection rate compared to all particles ($p < 0.001$, (Lenz et al., 2015)).

As a comparison a study collecting MP of sizes larger than 250 μm in the North East Atlantic west of Ireland (Lusher et al., 2014) found concentrations ranging from 0 to 22.5 m^{-3} with the mean at 2.5 m^{-3}, whereas our concentrations in the same size range were substantially higher with a mean of 44.6 m^{-3} and a range between 4 to 117 m^{-3}.

Comparing our S-MP dominated data set to a long-term series (20 years) of L-MP concentration measurements in the western part of the NASG (Law et al., 2010) reveals good consistency in distribution patterns. In particular the two stations of highest concentration (St. 23, 46) were identified as microplastic (L-MP) hotspot areas before.

A theoretical Lagrangian drifter model (Maximenko et al., 2012) shown in Fig. 12 predicted the accumulation of surface plastic in the NASG with an east-west expansion throughout the Atlantic between 25°N and 40°N over a timespan of 10 years emerging from an initially homogeneous state. The maximum MP concentrations in our study were located about 12° westward from the predicted maximum accumulation zones after 10 years.

Instead, our distribution pattern, shown in Fig. 12a, was better approximated by the solution after one year where the up-concentration of MP in the central gyre is not yet fully developed and two zones of accumulation can be observed: one in the western Sargasso Sea and a weaker one around the Azores (Fig. 12b). On the contrary, the spatial distribution of L-MP and larger plastic debris in the Northern Subtropical Atlantic was reported with maximum concentrations between 39° and 55° W (Cózar et al., 2014). Comparing their concentration distribution to the drift model prediction (Maximenko et al., 2012) it obviously is closer to the 10 years scenario (Fig. 12c). We argue that these differences in distribution patterns can be explained by a shorter residence time of S-MP in the surface layer. The resulting concentration profiles of our water column model supports this idea, showing an increased vertical distribution of microplastics with decreasing size, which dilutes S-MP abundances in surface ocean waters.

Fragmented microplastic is expected to initially occur concomitantly with its macroplastic precursors. In addition to this secondary microplastic formation in the gyres, coastal regions were identified as being

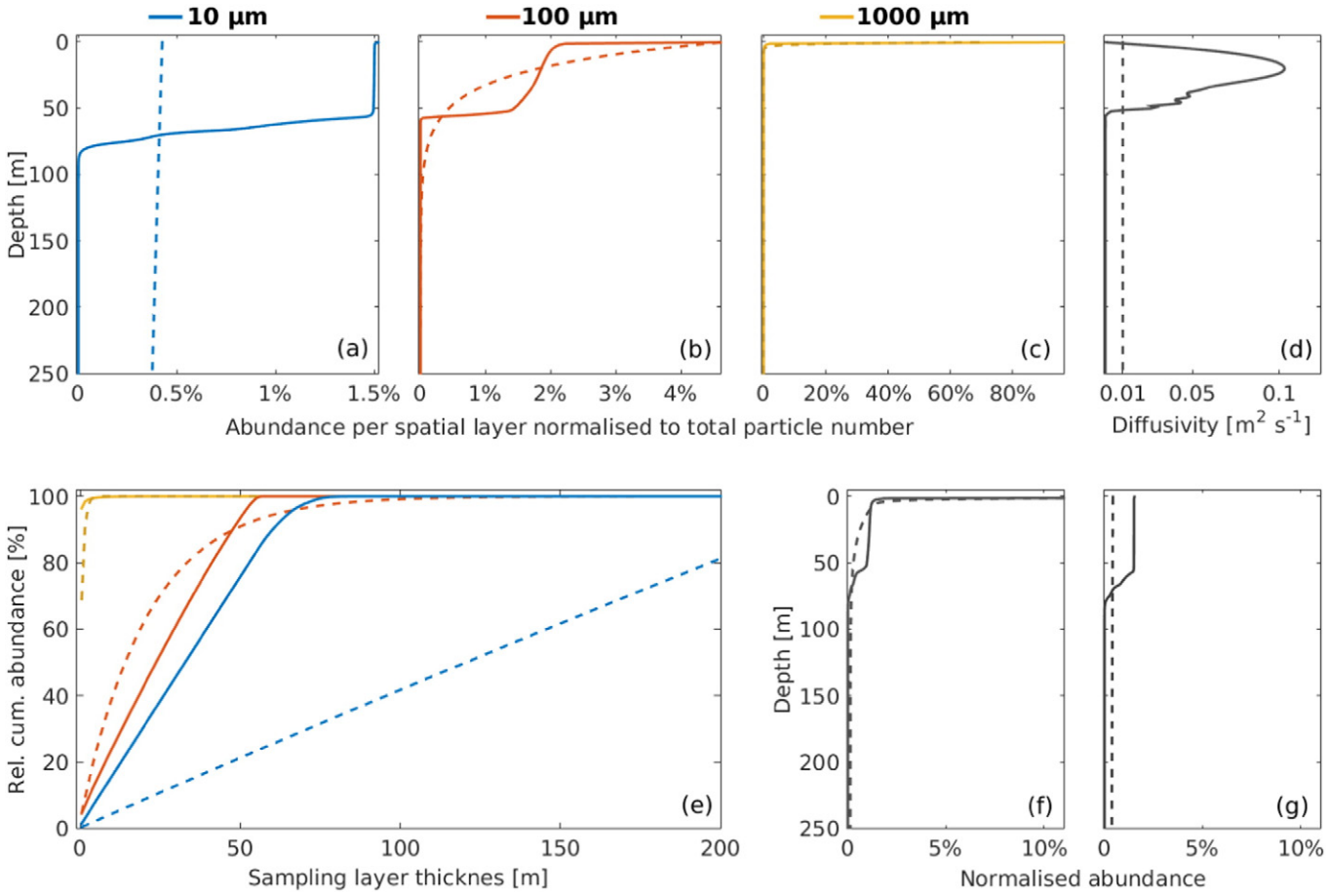

Fig. 10. Modelled vertical distribution of polyethylene MP in 3 sizes, approximated as equivalent spherical diameter (ESD). Particles were injected at initial conditions in the uppermost vertical layer (modelled domain depth 250 m, spatial resolution 1 m). Dashed lines represent a model case where a constant diffusivity vector was used. Solid line graphs were produced by using open ocean turbulence conditions, simulated in GOTM. (a–c) show the converged solutions with numbers normalised to the total number of particles in the water column. (d) applied diffusivity profiles. (e) cumulated plastic abundance from surface to possible sampling depths. (f) total plastic distribution with equal numbers of plastic spheres in each size class. (g) total plastic concentration with size-dependent initial conditions $N = ESD^{-3}$. Abundance axes in (f) and (g) were harmonised for better comparability. The actual maximum of (f) was at 34.4%.

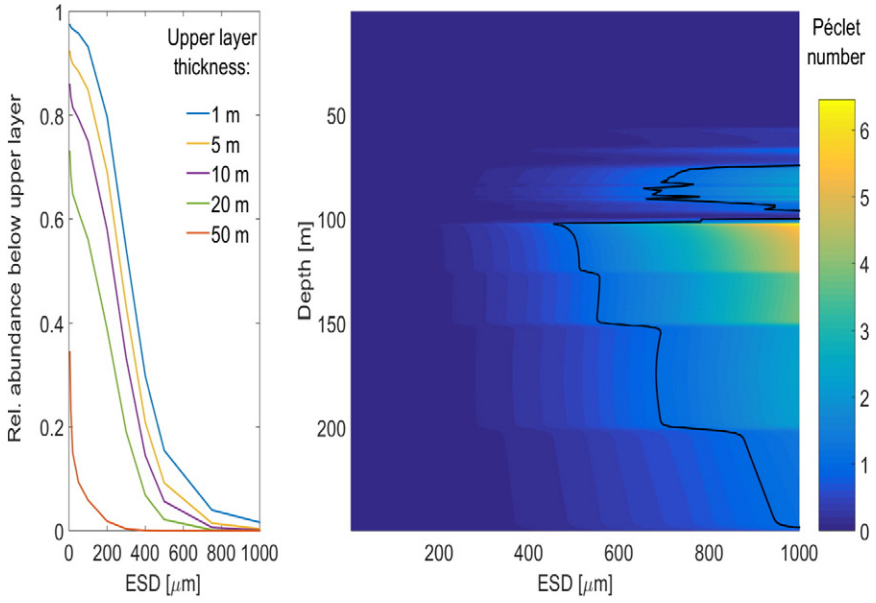

Fig. 11. (left) Size dependence of the portion of total plastic abundance that is mixed below the surface layer compartment for 5 different layer thicknesses. (right) Péclet number over size and depth. Black line indicates Pe = 1.

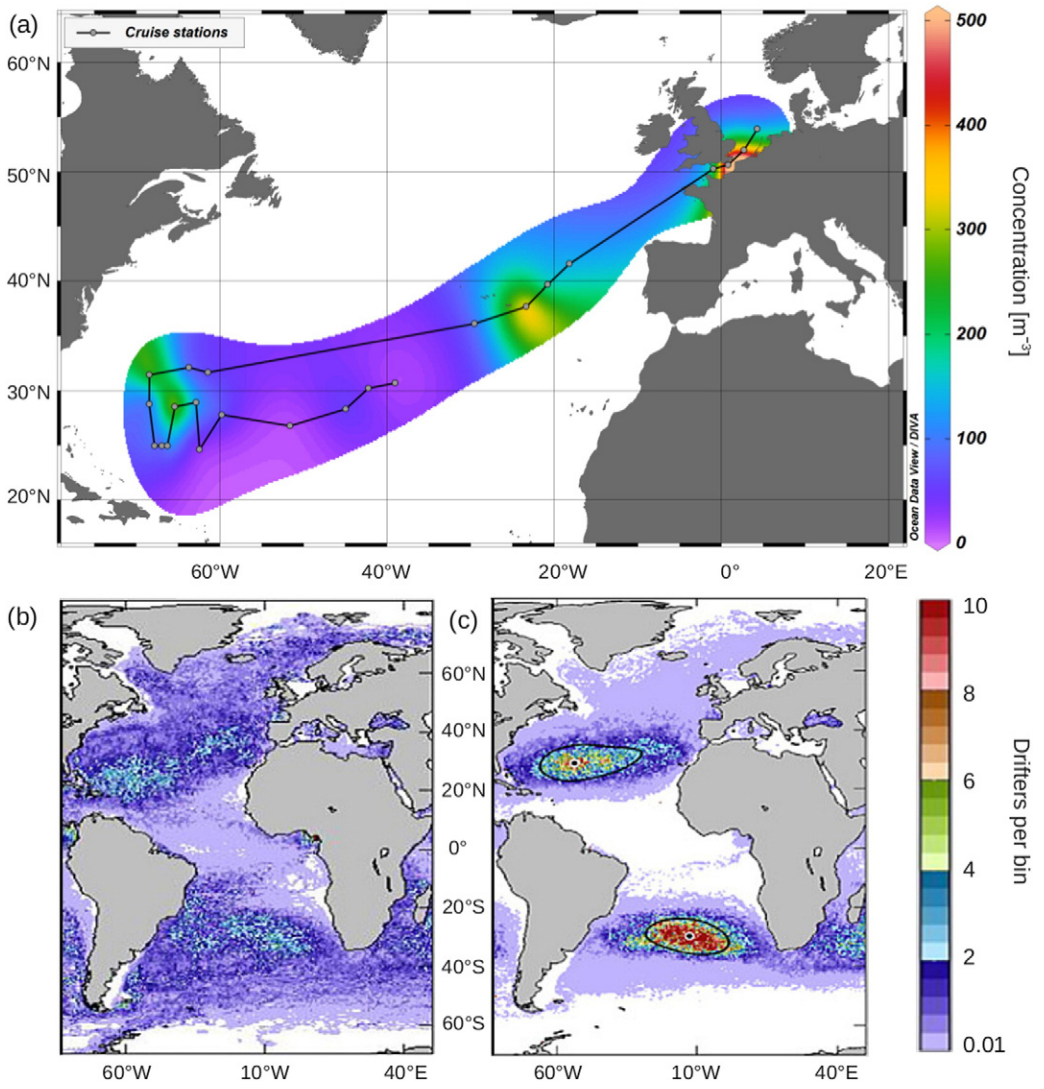

Fig. 12. Evaluation of the observed North Atlantic MP pattern under the perspective of oceanographic drift. Total MP concentrations ≥ 10 μm in the surface (a). Spatial gridded interpolation was created with the DIVA function in Ocean Data View 4 (Schlitzer, 2015). Below: maps showing the solution to a drift model simulating the spatial distribution of oceanic surface drifters: after 1 year (b) and 10 years (c). Maps (b) and (c) modified from (Maximenko et al., 2012).

a major contributor to fragmentation processes as a result of size-selective onshore mass transport of meso- and macroplastics (Isobe et al., 2014). The formed microplastics can to a large extent escape the onshore Stokes drift, which decays exponentially with depth, and return back offshore. Estuaries and semi-enclosed coastal regions can also act as accumulation zones with fragmentation conditions harsher than in the gyres, due to increased wave action and grinding by sand and rocks. Together with primary microplastics from land or shipping activities the input and net distribution of microplastics is rather dispersed in contrast to more point-like sources of macroplastic.

Over large spatial scales average microplastic concentrations decrease with distance from land due to dilution, implying that the major input comes from land. Over smaller scales concentrations are influenced by local sources and residence times. Hence, the elevated concentration that we found in the western part of the gyre may partially be influenced from coastal plastic loads from the American continental coast, which was about 800 km from our most westward stations. The local concentration maximum at station 8 is most likely due to the proximity to the Azores islands (approx. 100 km) and consequent land based sources. The region is also characterised by intensive shipping activities.

In the NASG we measured highest MP concentrations in the mid latitudinal region, M-NASG, which were dominated by LD polymers. At the same time the contribution of HD was lowest of all regions. This is reasonable as the water here is considered relatively old in terms of last contact to land-based sources, thus time long enough for HD particles to sink out of the upper layer. All stations of M-NASG were situated in the frontal system. The northern and southern water masses bordering in this region converge at the frontal system leading to a downwelling which leaves behind transported plastic debris that is able to withstand the downward advection. This process would lead to increased plastic accumulation in the sea surface (Lebreton et al., 2012; Kukulka et al., 2012) which can be confirmed here regarding the elevated LD particle concentrations. On the other hand downwelling removes a part of the MP pool, preferentially small particles and MP of higher density that could only remain in the surface through turbulent mixing. In conformity with this, a study on S-MP in the Northern Pacific observed the opposite trend for a local upwelling region (Desforges et al., 2014) concluding that MP abundance is shaped by oceanographic conditions. Plastic particles with lower density will in average withstand the removal especially in the larger size ranges. Our data supports this theory as we find the strongest separation between HD and LD polymers

both in concentration and size in the M-NASG and the neighbouring N-NASG region.

Although our model did not support to find HD polymers in the surface ocean, they were present in our field samples, which were identified by Raman spectrometry. Also other studies reported PS, PES, PVC, and PA in sea surface or subsurface samples (Song et al., 2014; Norén et al., 2014; Chae et al., 2014). It is likely that other factors than terminal velocity and turbulent mixing play a role in the prevalence of various polymer types in sea surface. Biofilm formation and degradation may change the apparent density. Some macroplastic debris of heavy polymers may float due to air enclosures, i.e. foamed materials, thus providing a steady source at the sea surface of S-MP shred off by fragmenting physical and chemical forces. Furthermore, airborne microplastic can be introduced with dust from civilised areas. The above mentioned factors are possible reasons explaining the presence of higher density polymers as a result from a steady input over large spatial scales.

For different polymers these sources also depend on their typical applications and areas of use. It is likely that PA enters the ocean directly as shreds from ropes and nets used in shipping and fishing industry. In the M-NASG region fibrous microplastic was three times as abundant as particles. It has been empirically shown that vertical advection velocities are lowest for fibrous shaped microplastics compared to sheets and particles with otherwise equal properties (Ballent et al., 2012; Reisser et al., 2015). This contributes to fibres having longer residence times and thereby a more homogeneous horizontal concentration distribution in the upper layers of the water column. The most produced synthetic fibres are made from PES (Cho, 2007). Yet, due to its high density it is of overall low numeric abundance (6%, Fig. 8) and has its absolute minimum in the AOO region. PS was found equally spread across regions which may be due its small density difference to that of sea water. Additionally, expanded PS (EPS) can travel far before trapped air is released due to degradation processes, leading to a more dispersed occurrence PS micro-particles.

The size structure of MP particles was steadily increasing in numbers towards lower sizes and we could not confirm reduced amounts close to the lower sampling size, as several other studies reported (Cózar et al., 2014; Lusher et al., 2014; Morét-Ferguson et al., 2010). The number of particles, however, increased less than expected for a mass conserving fragmentation process, which is in conformity with a suggested 'missing fraction' of small sized MP (Cózar et al., 2014; Reisser et al., 2015). The smaller size classes (10 to 50 μm) therefore comprised a lower fraction of the total plastic load, compared to those in mid size range. A part of the missing particles in the 10 - 20 μm range can be explained by the diagonal of the filter meshes being about 14 μm leading to a partial slip through. The power law regressions to the size distributions suggest that fibres followed the expected one-dimensional fragmentation.

The group of particles included flat sheet-like fragments which are expected to increase in numbers squared with the decay of their size through fragmentation. However, the group will be dominated by three-dimensional fragmenting objects when fragments become very small and the theoretical scaling exponent can be expected to be close to 3 unless flat objects outnumber the three-dimensional particles, which was not the case in our samples. The fitted regression for this group was scaling with an exponent of 1.96, indicating that either fragmentation accelerates with decreasing size or that there is an effect of other loss terms, or a combination of both. In Table 2 we summarise the most important factors that contribute to the apparent loss of S-MP from the ocean surface layer. In accordance with this, size distribution of fibres found in the present study showed an abrupt decrease of sizes smaller 100 μm, which is most likely due to the fact that most fibres have a diameter ranging from 8–20 μm, which is close to the sample minimum. Thus the risk of slippage through the net is increased the shorter the fibre. Additionally, fibres of lengths close to their widths can be easily identified as particles instead.

Due to wind-induced mixing in within the upper layer of the water column, net tow sampling (usually at 0–25 cm depth) varies with strength of wind forcing where lower surface concentrations are generally associated with higher wind speeds (Kukulka et al., 2012). Under the limitations of a relatively small sample size no apparent trend between our plastic concentrations and wind speed is evident (Fig. 7), leading to the conclusion that underway water sampling is relatively insensitive to concentration under- or overestimation by wind induced mixing. This supports the assumption that underway water sampling collects a mixture of the upper water column (3 m), resulting in an homogeneously distributed sample representative. Similarly, plastic type composition shows a more diverse spectrum including various polymers denser than seawater, compared to net tow sampling activities (Isobe et al., 2014) and studies investigating on the upper end of the microplastic size spectrum (Reisser et al., 2015).

Given the vertical distribution dynamics, microplastics reaching greater depth are decreasingly influenced by surface currents and become subjected to other loss terms than floating debris. Attachment to marine snow as well as ingestion and subsequent removal by faecal pellets (Cole et al., 2013) are processes acting on an ocean wide scale, potentially leading to an acceleration of MP sinking rates of up to hundreds of metres per day. For comparison free 2 μm polystyrene beads ($\rho_{PS} = 1.05$ g cm^{-3}) reach sinking rates of 4 mm day^{-1} (Long et al., 2015). As marine snow constitutes the major source of carbon to filter feeders, given the higher MP loading interactions rates of MP to the organism are likely to increase with increasing S-MP pollution (Long et al., 2015).

Table 2
Loss terms explaining the 'missing' lower size fraction of MP. References are provided if loss terms were also discussed in other studies.

Methodology	Slippage through mesh by shortest dimension	
	Only reporting of longest dimension shifts size spectrum to larger sizes	
	Analysis inaccuracies at lower size limit	
	Differences in size composition depending on sampling depth	
Dynamics	Ingestion by marine biota	Law et al. (2010); Cózar et al. (2014)
	Incorporation in marine snow	Long et al., 2015
	Egested MP in sinking faecal pellets	Cole et al. (2013)
Fragmentation	(Nano-)fragmentation below detection size	Cózar et al. (2014)
	Size dependency of fragmentation rates	Cózar et al. (2014)

5. Conclusion

Based on the experiences with the applied sampling and analysis techniques we recommend the further development of ship underway sampling as well as Raman micro-spectrometry, which both have the potential to be useful tools in microplastic research especially when the numerous small sizes are targeted.

Our field and modelling results show that, once microplastic fragmented down to a certain size, rather dispersed distribution patterns can be observed, both horizontally as well as vertically. From this finding we conclude that the residence time of S-MP in the surface ocean must be considerably lower. The primarily physically and chemically governed processes of dilution and diffusion are accompanied by biological factors which predominantly act on small-sized MP and lead to further draw-down of the polymers into the ocean interior.

As an outlook, plastic marine debris is predicted to grow by an order of magnitude during the next decade as the amount of mismanaged plastics is directly proportional to the growing world population (Jambeck et al., 2015). This emphasises the importance to understand load, transport and degradation of, not only macro-, but microplastics in order to uncover the plastic cycle in the marine environment.

Acknowledgements

We thank Eik Ehlert Britsch and Magnus Bohr, which contributed to the sample collection and Peter Munk for excellent logistics and organisation of the expedition. Thanks to Jakob Strand from Aarhus University who kindly provided the melting apparatus. The Raman microscope was provided by David Mackenzie and Peter Bøggild from DTU Nanotech. We acknowledge the helpful suggestions of Ken Andersen in the modelling part. The research was funded by DTU Aqua, Carlsberg Foundation (2012-01-0272) and the Danish Center for Marine Research (2013-02).

References

Andrady, A.L., 2003. Plastics and the environment. John Wiley & Sons, Inc., Hoboken, New Jersey.

Andrady, A.L., 2011. Microplastics in the marine environment. Mar. Pollut. Bull. 62 (8), 1596–1605. http://dx.doi.org/10.1016/j.marpolbul.2011.05.030.

Avio, C.G., Gorbi, S., Milan, M., Benedetti, M., Fattorini, D., D'Errico, G., Pauletto, M., Bargelloni, L., Regoli, F., 2015. Pollut ants bioavailability and toxicological risk from microplastics to marine mussels. Environ. Pollut. 198, 211–222. http://dx.doi.org/10.1016/j.envpol.2014.12.021 (URL http://linkinghub.elsevier.com/retrieve/pii/S0269749114005211).

Ballent, A., Purser, A., de Jesus Mendes, P., Pando, S., Thomsen, L., 2012. Physical transport properties of marine microplastic pollution. Biogeosci. Discuss. 9, 18755–18798. http://dx.doi.org/10.5194/bgd-9-18755-2012 (URL http://www.biogeosciences-discuss.net/9/18755/2012/).

Boyd, C.M., 1976. Selection of particle sizes by filter-feeding copepods: a plea for reason. Am. Soc. Limnol. Oceanogr. 21 (1), 175–180.

Burchard, H., Bolding, K., Villarreal, M.R., 1999. GOTM, a general ocean turbulence model: theory, implementation and test cases. Tech. rep., EUR 18745 EN.

Chae, D.-H., Kim, I.-S., Song, Y.K., Kim, S., Kim, S.-K., 2014. Development of analytical method for microplastics in seawater. Sea 19 (1), 88–98. http://dx.doi.org/10.7850/jkso.2014.19.1.88 (URL http://ocean.kisti.re.kr/IS_mvpopo001P.do?method=multMain&cn1=JAKO201408739558303&poid=ksoc&free=).

Cho, L.L., 2007. Identification of textile fiber by Raman microspectroscopy. Forensic Sci. J. 6 (1), 55–62 (URL http://scholar.google.com/scholar?hl=en&btnG=Search&q=intitle:Identification+of + textile + fiber + by + Raman + microspectroscopy#1).

Cole, M., Lindeque, P., Fileman, E., Halsband, C., Galloway, T.S., 2015. The Impact of Polystyrene Microplastics on Feeding, Function and Fecundity in the Marine Copepod Calanus helgolandicus. Environ. Sci. Technol. http://dx.doi.org/10.1021/es504525u URL http://www.ncbi.nlm.nih.gov/pubmed/25563688.

Cole, M., Lindeque, P., Halsband, C., Galloway, T.S., 2011. Microplastics as contaminants in the marine environment: a review. Mar. Pollut. Bull. 62 (12), 2588–2597. http://dx.doi.org/10.1016/j.marpolbul.2011.09.025 (URL http://www.ncbi.nlm.nih.gov/pubmed/22001295).

Cole, M., Lindeque, P., Fileman, E., Halsband, C., Goodhead, R., Moger, J., Galloway, T.S., 2013. Microplastic ingestion by zooplankton. Environ. Sci. Technol. 47 (12), 6646–6655. http://dx.doi.org/10.1021/es400663f (URL http://www.ncbi.nlm.nih.gov/pubmed/23692270).

Costa, M.F., Ivar do Sul, J.A., Silva-Cavalcanti, J.S., Araújo, M.C.B., Spengler, A., Tourinho, P.S., 2010. On the importance of size of plastic fragments and pellets on the strandline: a snapshot of a Brazilian beach. Environ. Monit. Assess. 168 (1-4), 299–304. http://dx.doi.org/10.1007/s10661-009-1113-4 (URL http://www.ncbi.nlm.nih.gov/pubmed/19680758).

Cózar, A., Echevarria, F., Gonzalez-Gordillo, J.I., Irigoien, X., Ubeda, B., Hernandez-Leon, S., Palma, A.T., Navarro, S., Garcia-de Lomas, J., Ruiz, A., Fernandez-de Puelles, M.L., Duarte, C.M., 2014. Plastic debris in the open ocean. Proc. Natl. Acad. Sci. 111 (28), 10239–10244. http://dx.doi.org/10.1073/pnas.1314705111 (URL http://www.pnas.org/cgi/doi/10.1073/pnas.1314705111).

Desforges, J.P.W., Galbraith, M., Dangerfield, N., Ross, P.S., 2014. Widespread distribution of microplastics in subsurface seawater in the NE Pacific Ocean. Mar. Pollut. Bull. 79 (1–2), 94–99. http://dx.doi.org/10.1016/j.marpolbul.2013.12.035 URL http://www.ncbi.nlm.nih.gov/pubmed/24398418.

Eriksen, M., Lebreton, L.C.M., Carson, H.S., Thiel, M., Moore, C.J., Borerro, J.C., Galgani, F., Ryan, P.G., Reisser, J., 2014. Plastic pollution in the world's oceans: more than 5 trillion plastic pieces weighing over 250,000 tons afloat at sea. PLoS ONE 9 (12), e111913. http://dx.doi.org/10.1371/journal.pone.0111913.

Isobe, A., Kubo, K., Tamura, Y., Kako, S., Nakashima, E., Fujii, N., 2014. Selective transport of microplastics and mesoplastics by drifting in coastal waters. Mar. Pollut. Bull. 89 (1-2), 324–330. http://dx.doi.org/10.1016/j.marpolbul.2014.09.041 (URL http://linkinghub.elsevier.com/retrieve/pii/S0025326X1400650X).

Ivar do Sul, J.A., Costa, M.F., 2014. The present and future of microplastic pollution in the marine environment. Environ. Pollut. (Barking, Essex: 1987) 185, 352–364. http://dx.doi.org/10.1016/j.envpol.2013.10.036 (URL http://www.ncbi.nlm.nih.gov/pubmed/24275078).

Jambeck, J.R., Geyer, R., Wilcox, C., Siegler, T.R., Perryman, M., Andrady, A., Narayan, R., Law, K.L., 2015. Plastic waste inputs from land into the ocean. Science.

Kiørboe, T., Andersen, A., Langlois, V.J., Jakobsen, H.H., 2010. Unsteady motion: escape jumps in planktonic copepods, their kinematics and energetics. J. R. Soc. Interface/R. Soc. 7 (52), 1591–1602. http://dx.doi.org/10.1098/rsif.2010.0176.

Kukulka, T., Proskurowski, G., Morét-Ferguson, S., Meyer, D.W., Law, K.L., 2012. The effect of wind mixing on the vertical distribution of buoyant plastic debris. Geophys. Res. Lett. 39 (7). http://dx.doi.org/10.1029/2012GL051116 (n/a–n/a, URL http://doi.wiley.com/10.1029/2012GL051116).

Law, K.L., Morét-Ferguson, S., Maximenko, N.A., Proskurowski, G., Peacock, E.E., Hafner, J., Reddy, C.M., 2010. Plastic accumulation in the North Atlantic subtropical gyre. Science (New York, N.Y.) 329 (5996), 1185–1188. http://dx.doi.org/10.1126/science.1192321 (URL http://www.ncbi.nlm.nih.gov/pubmed/20724586).

Lebreton, L.C.-M., Greer, S.D., Borrero, J.C., 2012. Numerical modelling of floating debris in the world's oceans. Mar. Pollut. Bull. 64 (3), 653–661. http://dx.doi.org/10.1016/j.marpolbul.2011.10.027 (URL http://www.ncbi.nlm.nih.gov/pubmed/22264500).

Lee, H., Shim, W.J., Kwon, J.-H.H., 2014. Sorption capacity of plastic debris for hydrophobic organic chemicals. Sci. Total Environ. 470-471, 1545–1552. http://dx.doi.org/10.1016/j.scitotenv.2013.08.023 (URL http://www.ncbi.nlm.nih.gov/pubmed/24012321).

Lenz, R., Enders, K., Stedmon, Colin A., Mackenzie, David M.A., Nielsen, Torkel Gissel, 2015. A critical assessment of visual identification of marine microplastics using raman spectroscopy for analysis improvement. http://dx.doi.org/10.1016/j.marpolbul.2015.09.027.

Long, M., Moriceau, B., Gallinari, M., Lambert, C., Huvet, A., Raffray, J., Soudant, P., 2015. Intera ctions between microplastics and phytoplankton aggregates: Impact on their respective fates. Mar. Chem. http://dx.doi.org/10.1016/j.marchem.2015.04.003 URL http://linkinghub.elsevier.com/retrieve/pii/S0304420315000766.

Lusher, A.L., Burke, A., O'Connor, I., Officer, R., 2014. Microplastic pollution in the Northeast Atlantic Ocean: Validated and opportunistic sampling. Mar. Pollut. Bull. 88 (1–2), 325–333. http://dx.doi.org/10.1016/j.marpolbul.2014.08.023 URL http://linkinghub.elsevier.com/retrieve/pii/S0025326X14005530.

Magnusson, K., 2013. Microscopic anthropogenic particles — methods for monitoring and results from a survey. (URL http://gesreg.msi.ttu.ee/download/20130206_KerstinMagnusson.pdf).

Maximenko, N., Hafner, J., Niiler, P., 2012. Pathways of marine debris derived from trajectories of Lagrangian drifters. Mar. Pollut. Bull. 65 (1-3), 51–62. http://dx.doi.org/10.1016/j.marpolbul.2011.04.016 (URL http://www.ncbi.nlm.nih.gov/pubmed/21696778).

Morét-Ferguson, S., Law, K.L., Proskurowski, G., Murphy, E.K., Peacock, E.E., Reddy, C.M., 2010. The size, mass, and composition of plastic debris in the western North Atlantic Ocean. Mar. Pollut. Bull. 60 (10), 1873–1878. http://dx.doi.org/10.1016/j.marpolbul.2010.07.020 (URL http://www.ncbi.nlm.nih.gov/pubmed/20709339).

Norén, F., 2007. Small plastic particles in Coastal Swedish waters. Tech. Rep. 0, KIMO.

Norén, F., Naustvol, L.-J., 2010. Survey of microscopic anthropogenic particles in Skagerrak. Tech. Rep. Institute of Marine Research, Flø devigen November.

Norén, F., Naustvoll, L.-J., 2011. Pilot study: survey of microscopic anthropogenic particles in Skagerrak. Tech. Rep. Klima-og Forurensningsdirektoratet: TA2779/2011. N-research and Havforskningsinstituttet, Lysekil, Sweden.

Norén, F., Norén, K., Magnusson, K., 2014. Marint mikroskopiskt skräp Undersökning längs svenska västkusten. Tech. rep.

Reisser, J., Slat, B., Noble, K., du Plessis, K., Epp, M., Proietti, M., de Sonneville, J., Becker, T., Pattiaratchi, C., 2015. The vertical distribution of buoyant plastics at sea: an observational study in the North Atlantic Gyre. Biogeosciences 12, 1249–1256. http://dx.doi.org/10.5194/bg-12-1249-2015 (URL http://www.biogeosciences.net/12/1249/2015/).

Rocha-Santos, T., Duarte, A.C., 2014. A critical overview of the analytical approaches to the occurrence, the fate and the behavior of microplastics in the environment. TrAC Trends Anal. Chem. 65, 47–53. http://dx.doi.org/10.1016/j.trac.2014.10.011 (URL http://linkinghub.elsevier.com/retrieve/pii/S0165993614002556).

Rochman, C.M., 2013. Plastics and priority pollutants: a multiple stressor in aquatic habitats. Environ. Sci. Technol. 47 (6), 2439–2440. http://dx.doi.org/10.1021/es400748b (URL http://www.ncbi.nlm.nih.gov/pubmed/23452158).

Schlitzer, R., 2015. Ocean Data View, ODV.

Song, Y.K., Hong, S.H., Jang, M., Kang, J.-H., Kwon, O.Y., Han, G.M., Shim, W.J., 2014. Large accumulation of micro-sized synthetic polymer particles in the sea surface microlayer. Environ. Sci. Technol. 48, 9014–9021. http://dx.doi.org/10.1021/es501757s (URL http://www.ncbi.nlm.nih.gov/pubmed/25059595).

Song, Y.K., Hong, S.H., Jang, M., Han, G.M., Rani, M., Lee, J., Shim, W.J., 2015. A comparison of microscopic and spectroscopic identification methods for analysis of microplastics in environmental samples. Mar. Pollut. Bull. 1–8 http://dx.doi.org/10.1016/j.marpolbul.2015.01.015 (URL http://linkinghub.elsevier.com/retrieve/pii/S0025326X15000314).

Stuart, B.H., 2002. Polymer analysis, Sydney.

Ullman, D.S., Cornillon, P.C., Shan, Z., 2007. On the characteristics of subtropical fronts in the North Atlantic. J. Geophys. Res. Oceans 112 (1), C01010. http://dx.doi.org/10.1029/2006JC003601 URL http://doi.wiley.com/10.1029/2006JC003601.

Umlauf, L., Burchard, H., Bolding, K., 2012. GOT M-sourcecode and test case documentation. (URL http://www.gotm.net/pages/documentation/manual/stable/pdf/a4.pdf).